Exciton dynamics in self-assembled molecular nanotubes

Kriete, Björn

DOI:
10.33612/diss.123832795

Chapter 6

Steering Self-Assembly of Amphiphilic Molecular Nanostructures via Halogen Exchange

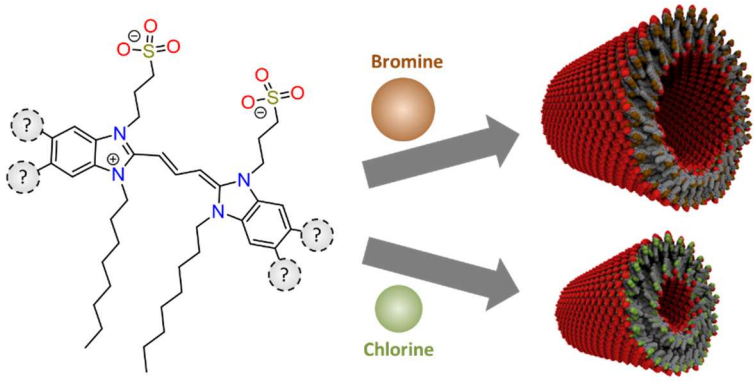

In the field of self-assembly, the quest for gaining control over the supramolecular architecture without affecting the functionality of the individual molecular building blocks is intrinsically challenging. By using a combination of synthetic chemistry, cryogenic transmission electron microscopy, optical absorption measurements, and exciton theory, we demonstrate that halogen exchange in carbocyanine dye molecules allows for fine-tuning the diameter of the self-assembled nanotubes formed by these molecules, while hardly affecting the molecular packing determined by hydrophobic/hydrophilic interactions. Our findings open a unique way to study size effects on the optical properties and exciton dynamics of self-assembled systems under well-controlled conditions.

This Chapter is based on the following publication:
Björn Kriete*, Anna S. Bondarenko*, Varsha R. Jumde*, Linda E. Franken, Adriaan J. Minnaard, Thomas L. C. Jansen, Jasper Knoester, and Maxim S. Pshenichnikov, *The Journal of Physical Chemistry Letters* **8**, 2895-2901 (2017); (*) denotes equal contributions

6.1 Introduction

Molecular self-assembly has proven to be a versatile tool in nanotechnology, as it allows for the autonomous and reproducible assembly of a wide variety of low-dimensional functional systems, extending in size from 10's of nanometers to microns[1]. A key challenge in the field of self-assembly is to control the shape and size of the final supramolecular structure with minimal changes of the molecular entities that provide the functionality essential for potential applications[2–4]. As the structure of the final assembly is encoded in each individual building block, any modification becomes a highly non-trivial task that requires fine-tuning at the molecular level. It has been shown that tailoring non-covalent molecular interactions such as π-stacking[5], hydrogen bonding[6], halogen bonding[7,8] or hydrophobic/hydrophilic interactions[9–11] provides powerful approaches in directing self-assembly. The coordinating nature of hydrophobic/hydrophilic interactions is of special interest, as it may be utilized to tune the supramolecular structure by solely changing the hydrophilic or hydrophobic side groups of the molecules without affecting their functional cores. Indeed, variations of size and composition of the amphiphilic substituents have been used to change between various structures, such as micelles and bilayers, which is often accompanied by changes in the molecular packing[12,13]. In this Chapter, we show that even more subtle modifications, namely just replacing a few halogen atoms, may be used to complement hydrophobic/hydrophilic interactions for fine control over the characteristic size of a self-assembled structure, while preserving the molecules' functional properties and their supramolecular packing.

We demonstrate this control of self-assembly for a class of tubular molecular nanotubes of amphiphilic carbocyanine molecules that recently have attracted considerable interest for their optical functionality[14–16]. The close packing of the optically active carbocyanine molecules within the nanotubes gives rise to efficient excitation energy transfer and collective optical effects caused by exciton states shared by many molecules[17]. Changing the amphiphilic side groups results in a wide variety of different supramolecular structures[18–22], of which double-walled tubular structures with a diameter in the order of 10 nm have attracted the most attention[23–29]. The strong interest in these tubular nanotubes stems from their structural resemblance to the light-harvesting antennae of photosynthetic green sulfur bacteria[30–34], which are the most efficient photosynthetic organisms known. Also, the potential of the tubular nanotubes as quasi-one-dimensional energy transport wires is of great interest. Previous attempts to control the diameter of tubular nanotubes, including changing solvents or adding surfactants yielded only limited variations of the diameter and often completely changed the supramolecular architecture[35–37], thereby impeding systematic studies of the size effect on the optical functionality and energy transport.

In this Chapter we show how the diameter of the double-walled tubular system may be increased in a well-defined fashion (by 40 % for the outer wall and 110 % for the inner one) by replacing the four chlorine atoms in the original carbocyanine molecule by bromine atoms. By measurement and simulation of the absorption spectrum, we show that radial inflation of this tubular system is achieved without significantly altering the molecular packing. Besides extending the toolbox of controlling self-assembly, our results pave the road to greater flexibility in controlling of the diameter of tubular nanotubes by e.g. partial substitution of the halogen atoms. This would provide a model system to elucidate the effects of the inherent structural heterogeneity (namely variation of the radii) encountered in natural chlorosomes[34]. Moreover, such systematic control also opens up unprecedented opportunities to study size effects on such important photonics properties as exciton

dynamics – a crucial aspect of efficient energy transport – and polarization properties, both equally intriguing from theoretical and experimental points of view[29,38–40].

6.2 Results and Discussion

The dye molecule of interest in this study is the new cyanine dye derivative 3,3′-bis(2-sulfopropyl)-5,5′,6,6′-tetrabromo-1,1′-dioctylbenzimidacarbocyanine, or C8S3-Br, as opposed to its commercially available and much studied counterpart C8S3-Cl (Figure 6.1). The new molecules were produced in a four-step synthesis described in detail in the experimental section and the supplementary information of the published paper[41].

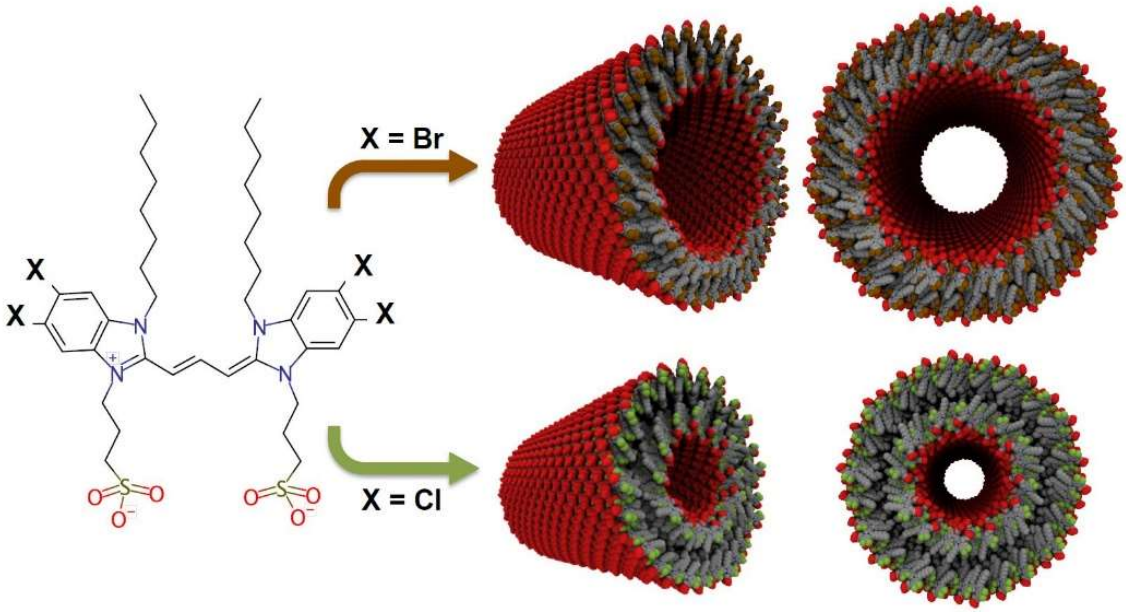

Figure 6.1. Chemical structure of C8S3. The halogen substituents are abbreviated as X = Br (C8S3-Br) and X = Cl (C8S3-Cl). The right panels illustrate differences in aggregate architectures formed by changing the halogen substituent from chlorine to bromine, as revealed by this work.

Exchanging chlorine with bromine slightly shifts the absorption peak of diluted molecules towards longer wavelengths, but introduces no other new features (Figure 6.2a), which is in line with our electronic structure calculations[41]. Addition of Milli-Q water to the methanolic C8S3-Br/Cl stock solutions induces a spectral red-shift of about 75 nm ($\sim$2400 cm^{-1}) and narrowing of absorption and photoluminescence (PL) bands, both features that are typical for J-type aggregation (Figure 6.2a).

The two sharp low-energy bands that both nanotube spectra have in common are broader for C8S3-Br than for C8S3-Cl. In addition, the high-energy flank of the C8S3-Br nanotube spectrum misses the peaks at $\sim$560 nm and $\sim$570 nm characteristic for the C8S3-Cl nanotube spectrum. Because the optical properties of molecular aggregates are governed by the interplay of all individual building blocks, the question arises what changes in the nanotube morphology induced by the halogen substitution are responsible for the observed spectral changes.

Experimental evidence for the aggregation of molecules into nanotubes, as schematically depicted in Figure 6.1, was found by cryo-TEM. Although thicker bundles of C8S3-Br were occasionally observed (SI, Section 6.5.1), there was no apparent morphological relation with the isolated tubes. Therefore, the more abundant nanotubes will be the focus of this study.

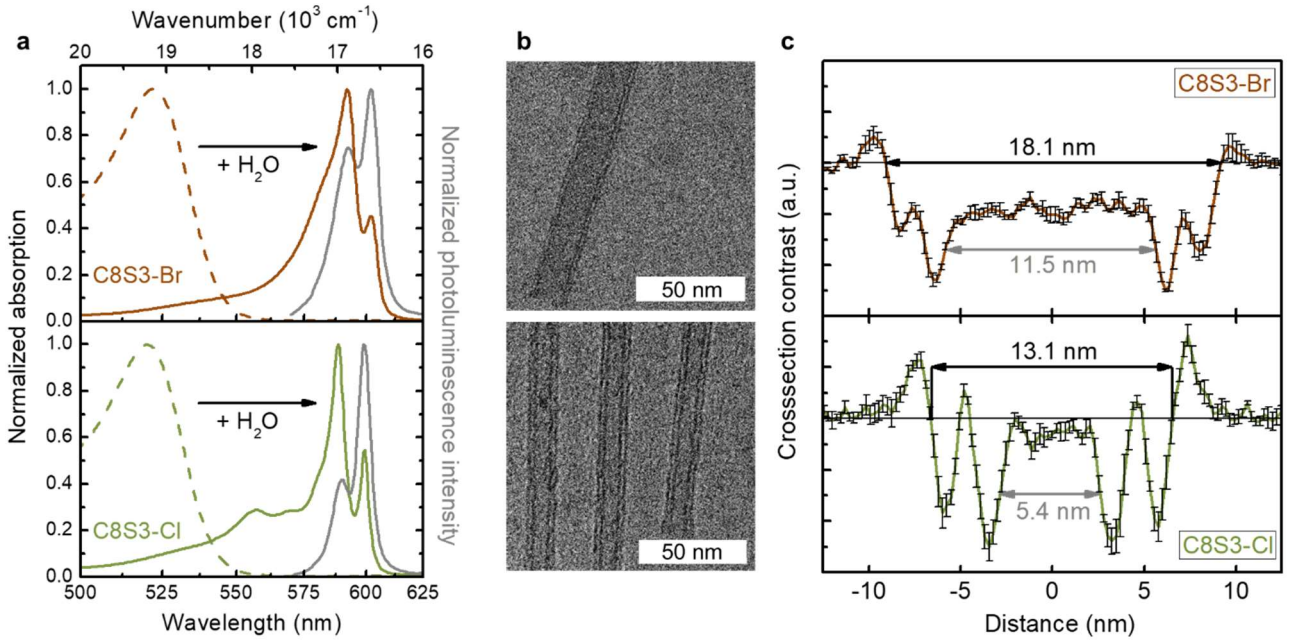

Figure 6.2. (a) Absorption (solid lines) and PL (solid grey) spectra of molecular nanotubes of C8S3-Br (top panel) and C8S3-Cl (bottom panel). Absorption spectra of both molecules diluted in methanol are shown for comparison (dashed lines). For collecting the PL spectra, the excitation wavelength was set to 560 nm. (b) Representative cryo-TEM micrographs for C8S3-Br (upper panel) and C8S3-Cl (lower panel) nanotubes illustrate the double-walled structure. (c) Profile scans for C8S3-Br (brown) and C8S3-Cl (green) nanotubes, obtained by integrating the signal along the tube axis. The characteristic sizes of the nanotubes are indicated by black and grey arrows for the outer and inner cylinder, respectively. The error bars represent the standard error upon averaging individual profile scans. For both C8S3-Cl and C8S3-Br five straight nanotube segments were used for averaging. The total length over which the profile was integrated amounts to approximately 200 nm and 400 nm for C8S3-Cl and C8S3-Br, respectively.

The cryo-TEM micrograph in Figure 6.2b (top) clearly reveals a double-walled structure of C8S3-Br nanotubes, similar to the structure of the C8S3-Cl nanotubes (Figure 6.2b, bottom). The profile scans of the nanotubes are shown in Figure 6.2c from which the outer- and inner-wall diameters of C8S3-Br nanotubes are obtained as 18.1 ± 0.2 nm and 11.2 ± 0.3 nm, respectively. This is in striking difference with C8S3-Cl nanotubes, where these quantities are 13.1 ± 0.2 nm and 5.4 ± 0.1 nm, respectively. Accordingly, the wall-to-wall thickness of C8S3-Br nanotubes amounts to 3.4 ± 0.3 nm, which is thinner than for C8S3-Cl nanotubes (3.9 ± 0.1 nm). All error margins refer to the standard error upon averaging.

It is important to understand whether the changes in the absorption spectra (Figure 6.2a) are due mainly to the changes in diameter, or whether they result from different molecular packing in both types of nanotubes, which results in differences in excitonic interactions. Since the cryo-TEM micrographs lack sufficient signal and 3D analysis to enhance the signal-to-noise ratio requires prior information on the symmetry, we retrieve the molecular packing by simulating the absorption spectrum for model structures and determining the structural parameters by fitting the experimental spectrum.

As the basic framework, we use the Extended Herringbone (EHB) model, which successfully describes the optical transitions of the double-walled tubular nanotubes of C8S3-Cl[24]. Briefly (see SI of the published paper for more details; Ref. [41]), within the EHB model the molecular positions and orientations are obtained by starting from a rectangular planar lattice of molecules (transition dipoles parallel and in-plane). The molecules are alternately rotated over an angle $\pm\delta$ along their axis

(coincident with the transition dipole orientation) and alternately tilted out-of-plane over an angle $\pm\beta$. The lattice is then rolled onto a cylindrical surface over a chiral vector with length equal to the cylinder circumference and direction determined by its angle θ relative to the axis x of the plane (Figure 6.3). This results in a cylindrical nanotube structure with each unit cell containing two molecules, which in turn leads to four (two Davydov-split) optically dominant exciton transitions per cylinder[42]. The inner and outer cylinders were modeled as spectroscopically independent entities (SI, Sections 6.5.2 and 6.5.3 for justification), keeping the structural parameters similar for both cylinders, but varying the radii in accordance with the experimental values obtained from cryo-TEM measurements.

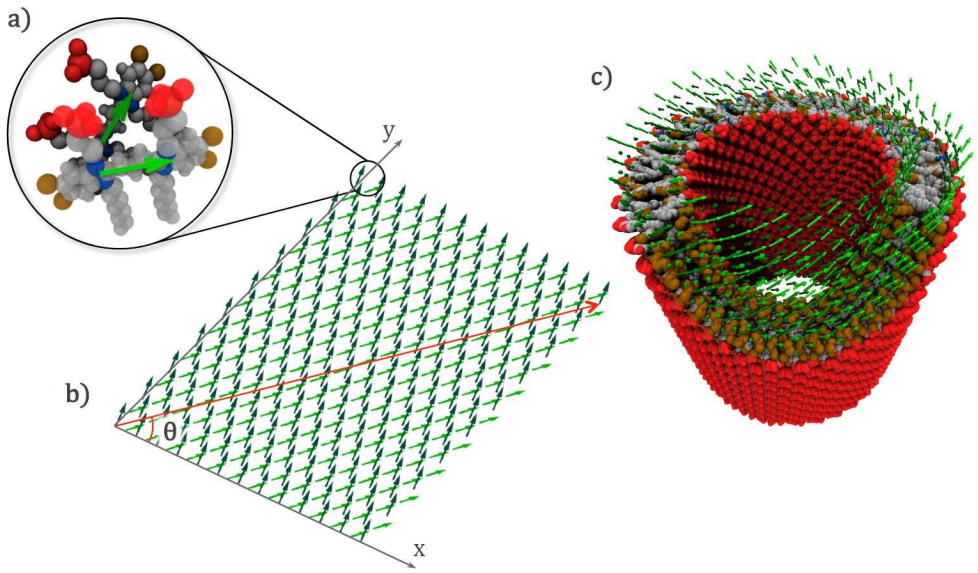

Figure 6.3. Schematic representation of the nanotube structure. The molecular pair (a) in each unit cell is shown above the two-dimensional molecular lattice (b). Two lattices are rolled along the chiral vectors (red arrow) to obtain the structure of the double-walled C8S3-Br nanotubes shown in (c), where transition dipole vectors are partially overlapped with the dye molecules.

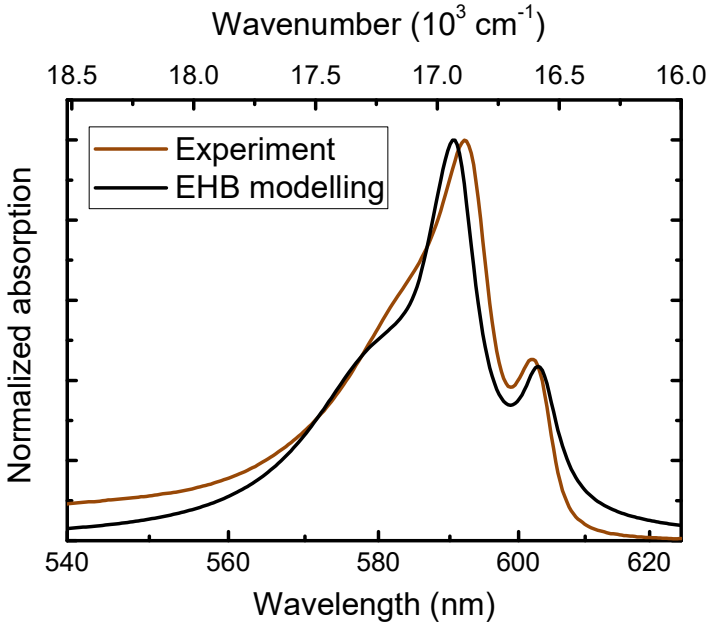

Figure 6.4. Comparison of the calculated absorption spectrum (black line) and the experimental one (brown line) for the double-walled tubular aggregate of C8S3-Br. The spectra are normalized to their respective peak values.

The lattice constants of the EHB model were taken identical to those for the C8S3-Cl case[24], while the free parameters β, δ, and θ that provide the best fit to the measured absorption spectrum for the C8S3-Br nanotubes are given in Table 6.1, along with the original parameters of C8S3-Cl[24] for comparison. Simulation of the absorption spectrum with these structural model parameters indeed gives a good reproduction of the experimental spectrum (Figure 6.4). In our modelling the lowest-energy peak near 600 nm is associated with the inner wall absorption (in close analogy to C8S3-Cl), while the higher-energy band has contributions from both walls. This spectral assignment of the inner and outer cylinder was verified in oxidation experiments[24,43,44] in which the absorption of the outer cylinder was impaired by silver nanoclusters (SI, Section 6.5.4). From Table 6.1, it appears that the molecular packing is essentially preserved upon the Cl → Br exchange, leaving the increase in the radii as the most important factor that changes the absorption spectrum, specifically the loss of the high-energy structure. In other words, the observed optical changes arise from an enhanced overlap of the excitonic transitions caused solely by the increase of the tube radius and not by changing the optical properties of the individual dyes or the packing of molecules within the supramolecular assembly.

Table 6.1. Summary of structural model parameters for the inner and outer walls of C8S3-Br used in the calculation of spectra (Figure 6.4) compared to the model of C8S3-Cl from Ref. [24]. The parameters β and δ define the lattice structure, while the parameter θ defines the aggregate lattice rolling.

	C8S3-Br		**C8S3-Cl**	
Parameter	Inner tube	Outer tube	Inner tube	Outer tube
r (nm)	6.50	8.61	3.55	6.47
β (°)	23.1	22.3	23.6	23.1
δ (°)	25.5	26.0	25.6	28.0
θ (°)	55.5	49.4	53.7	53.4

The modeling of the absorption spectra was performed in the homogeneous limit, i.e., all the molecular transition energies were assumed to be the same. As shown, this suffices to describe the absorption spectra and also explains the polarization properties of the spectral peaks (SI, Section 6.5.5 for linear dichroism), even though in reality some amount of disorder will occur in the transition energies and intermolecular resonance interactions. As has been shown by Bloemsma *et al.*[45], in tubular aggregates, such disorder leads to rather weak localization of the excitonic states, which explains the effectiveness of homogeneous models. Allowing for static Gaussian disorder in the transition energies[17,46] and assuming that this disorder solely determines the lowest energy aggregate band width, we find the maximum value (standard deviation) of the disorder to amount to 180 $\mathrm{cm^{-1}}$.

Above, the large spectral difference between C8S3-Cl and C8S3-Br (Figure 6.2a) was attributed to the change in radii of the inner and outer walls. This interpretation is further substantiated by phenomenologically examining the influence of the cylinder radii on the optical spectra. We modeled 12 cylinders based on the EHB lattice of the inner wall of C8S3-Cl (parameters in Table 6.1) by only varying the length of the rolling vector resulting in radii from 2.4 nm to 8.9 nm. For convenience of comparison (and in contrast to the fit in Figure 6.4), all spectral transitions were broadened by identical Lorentzian lineshapes of 120 $\mathrm{cm^{-1}}$ FWHM. The obtained spectra (Figure 6.5) reveal congestion of the peaks when going from the smallest cylinder with four well separated peaks to the largest cylinder with three peaks with little separation. Two peaks, the large one at 600 nm and the

small one at 570 nm, correspond to the doublet of transitions polarized parallel to the tube axis with their positions essentially independent of the radii. With increasing radius, the doublet of peaks with perpendicular polarization moves down in energy towards the parallel peaks, reflecting the fact that upon decreasing the cylinder curvature, the energy separation between corresponding parallel and perpendicular transitions decreases[15]. Consequently, with increasing cylinder radius, high-energy peaks vanish and spectral structure gets lost. In experiment, this effect is further enhanced by a stronger broadening of the higher-energy exciton peaks due to intraband relaxation, an effect not accounted for in Figure 6.5.

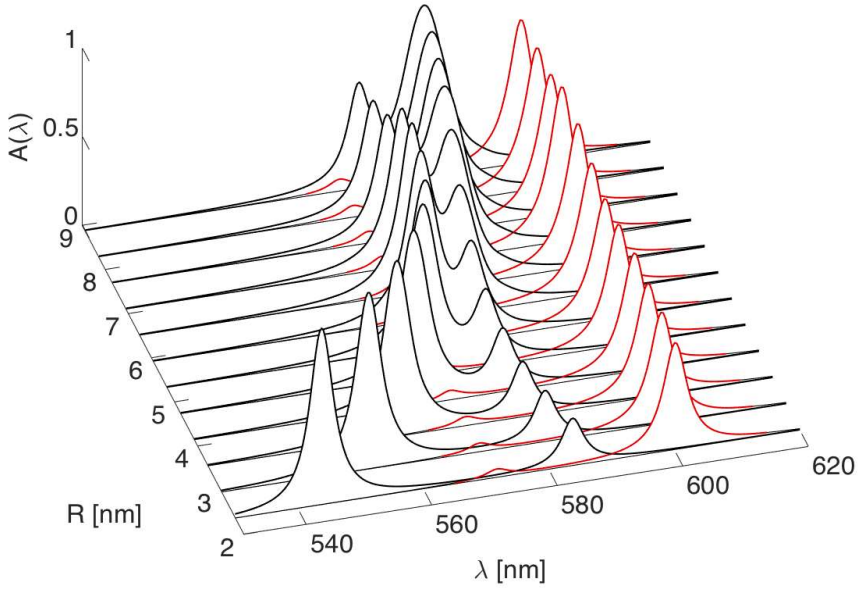

Figure 6.5. The influence of the tube radius on the absorption spectrum for a single tube with the EHB structure appropriate for the inner wall of C8S3-Cl nanotubes. Red and black lines correspond to the spectral components polarized parallel and perpendicular to the tube's axis, respectively. The spectral differences between R = 3.5 nm and R = 6.5 nm catch the essential differences between the spectra for the inner walls of C8S3-Cl and C8S3-Br.

6.3 Conclusions

In conclusion, we have shown that a very moderate chemical modification through the exchange of four halogen atoms in the chromophore of an amphiphilic carbocyanine dye leads to well-defined changes in the final supramolecular assembly without altering the underlying molecular architecture. This allowed us to study the effect of purely radial growth on the collective optical properties of the supramolecular structure. In a broader perspective, our results demonstrate that a combination of halogen exchange and amphiphilically driven self-assembly opens up unprecedented opportunities in controlling the supramolecular structure to a fine degree for systems, where modifications of other molecular moieties and/or changes of the immediate environment (solvent, pH, external fields) are not feasible as is the case in e.g. many biological systems or for medical applications. In addition, we believe that the presented design principle can be transferred to structurally related molecules that are known to form other supramolecular architectures, such as single-walled tubes[47], twisted bundles[19] or vesicles[19,35]. Nonetheless, the exact underlying mechanism of how halogen exchange affects the aggregation behavior is yet to be understood. Our results suggest that the size of the halogen substituents and/or the ability to form halogen bonds play an important role. For instance, fluorine, unlike bromine or chlorine, is known to hardly form halogen bonds and may even lead to intermolecular repulsion[8], which would impede the formation of molecular aggregates. We tested this

concept experimentally by synthesizing the C8S3-F molecule and indeed found a poor degree of aggregation under normal conditions (SI, Section 6.5.6). Based on our results, it is envisioned that further studies of partial replacement of only a few halogen atoms will shed light on the effect of different halogen substituents on the aggregation behavior. This would open great perspectives for fine-tuning size effects for optical functionality and for optimization of tubular aggregates for specific applications as for instance artificial light-harvesting systems.

6.4 Methods

6.4.1 Materials and Sample Preparation

The dye 3,3'-bis(2-sulfopropyl)-5,5',6,6-tetrachloro-1,1'-dioctylbenzimidacarbo-cyanine (C8S3-Cl, $M = 903\ \mathrm{g\,mol^{-1}}$) was purchased from FEW Chemicals GmbH (Wolfen, Germany) and used as received without further purification. Details on the synthesis and purification of the amphiphilic cyanine dye derivative 3,3'-bis(2-sulfopropyl)-5,5',6,6-tetrabromo-1,1'-dioctylbenzimidacarbo cyanine (C8S3-Br, $M = 1081\ \mathrm{g\,mol^{-1}}$) can be found in the published version of this Chapter[41].

Molecular nanotubes of the dyes were prepared via the alcoholic route[24]. The molecules were first dissolved in pure methanol (Biosolve) to form $1.75\ \mathrm{mM}$ stock solutions. In the next step the stock solution was added to Milli-Q water to induce aggregation and render a methanol content of $\sim 14\ \mathrm{wt\%}$ in the final sample solution. An immediate color change from orange to pink was detected by bare eye indicating the fast formation of J-aggregates due to hydrophobic solvent interactions. The resulting solution was gently shaken and stored in the dark at room temperature for days up to weeks for aggregation. The final dye concentration in the nanotube solution was $0.236\ \mathrm{mM}$.

6.4.2 Steady-State Absorption and Photoluminescence

Steady-state UV-Vis absorption spectra were measured using a PerkinElmer Lambda 900 UV/VIS/NIR spectrometer. For the pristine dyes diluted versions of the stock solutions were prepared with final dye concentrations in the range of $c = 10^{-4}\ \mathrm{M}$. Prior to measurements, sample solutions were diluted with Milli-Q water by factor 2. Steady-state PL spectra were recorded using a PerkinElmer LS50B Luminescence Spectrometer and $10\ \mathrm{mm}$ quartz cuvette (Starna GmbH, Germany). In order to avoid PL reabsorption, sample solutions were diluted with Milli-Q water by approximately factor 100.

6.4.3 Cryogenic Transmission Electron Microscopy

To prepare the samples for cryogenic transmission electron microscopy (cryo-TEM), a 3 µl droplet of the sample solution was placed on a copper grid with holey carbon film (quantifoil 3.5/1), which was first hydrophilized by glow discharging. In order to obtain a thin layer of the solution in the range of $100\ \mathrm{nm}$, the excess fluid was blotted off for $5\ \mathrm{s}$. Immediately afterwards the grid was vitrified in liquid ethane at its freezing point ($-184°\mathrm{C}$) with a Vitrobot (FEI, Eindhoven, The Netherlands). The grids were placed in a cryotransfer holder (Gatan model 626) and transferred into a Philips CM120 transmission electron microscope with an LaB6 cathode or a tungsten hairpin cathode operated at $120\ \mathrm{kV}$. Micrographs were recorded with an UltraScan 4000 UHS CCD camera (Gatan, Pleasanton, CA, USA) using low-dose mode.

6.4.4 Theoretical Calculations and Modeling

The geometry of each cylindrical tube of the double-walled tubular aggregate of C8S3-Br was obtained by rolling an EHB lattice with two molecules per unit cell[24]. The construction of the lattice and rolling procedure is briefly described in the main text and in detail in the SI of the published version of this Chapter[41]. All the input structural and energetic parameters were obtained either from previous studies[15,48,49] or obtained from the present cryo-TEM and optical experiments.

Optical electronic transitions were obtained by numerical diagonalization of the Frenkel exciton Hamiltonian[17] that accounts for molecular transition energies and Coulomb transfer interactions between the molecules with an extended dipole coupling model[15,48]. Coupling between the walls was neglected, allowing separate calculations for both walls. This approximation[24] is acceptable as the largest inter-wall couplings are significantly smaller than the intra-wall couplings and smaller than the homogeneous linewidth (SI, Section 6.5.2). The fitted spectrum was obtained in the homogenous limit where there is no disorder in the molecular transition energies. The obtained stick spectrum was broadened with Lorentzians of different width for the optimal agreement with experiment. More details are given in the SI of the published paper[41].

6.5 Supplementary Information

6.5.1 C8S3-Br Bundles

In occasional cases, the spontaneous formation of thicker bundles as illustrated in the cryo-TEM micrograph in Figure 6.6a was observed. The occurrence of the bundling could not be correlated with changes in preparation or age of the sample solution; hence we suspect residual contamination of the ingredients. The typical thickness of these bundles is in the range of 10's of nanometers and lengths are up to several micrometers. In addition, the thicker bundles often show a helical twist with a periodicity in the order of a few 100's of nanometers.

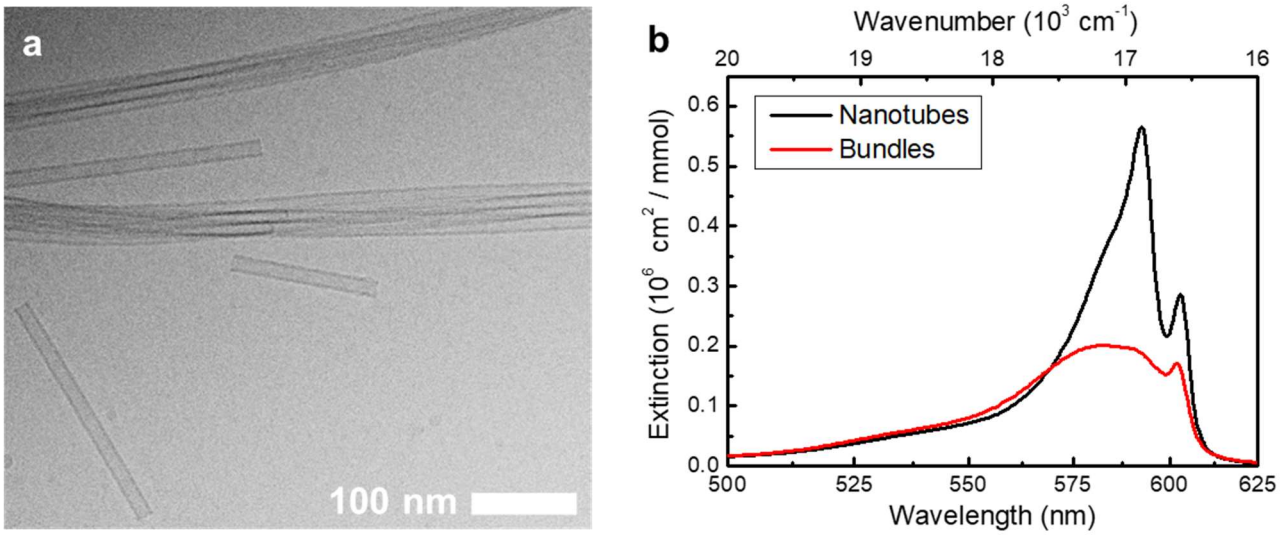

Figure 6.6. (a) Cryo-TEM micrograph of a 1 month old sample solution of C8S3-Br aggregates illustrating the co-existence of single aggregates and thicker bundles. (b) Linear absorption spectra of C8S3-Br nanotubes (black line) and bundles (red line).

The absorption spectrum that is associated with C8S3-Br bundles is shown in Figure 6.6b, which corresponds to an exceptional case where only bundles were observed. While the low energy peak could still be recognized, the high-energy peak is strongly suppressed. This provides a clear criterion to distinguish spectroscopically single nanotubes from bundles in experiment.

6.5.2 Intermolecular Couplings in C8S3-Cl and C8S3-Br Nanotubes

The largest inter-tube couplings in the C8S3-Br amount to $72\ \mathrm{cm}^{-1}$ compared to intra-tube couplings of $1500\ \mathrm{cm}^{-1}$. For C8S3-Cl the same numbers were $28\ \mathrm{cm}^{-1}$ and $1500\ \mathrm{cm}^{-1}$, respectively. While for C8S3-Br the inter-tube coupling is about $2-3$ times larger as for C8S3-Cl owing to the decreased tube separation, it is still significantly smaller than the intra-wall coupling. Moreover, the interwall couplings are smaller than the homogeneous linewidth of the exciton states, estimated as $200\ \mathrm{cm}^{-1}$. These values imply that the interwall couplings are too small to give rise to collective excitonic states shared by both walls, thus justifying our approach to model the system's absorption spectrum as the sum of the spectra of uncoupled inner and outer cylindrical walls. This conclusion is also supported by time-resolved PL measurements (SI, Section 6.5.3).

Table 6.2. The strongest positive and negative intermolecular couplings of C8S3-Cl and C8S3-Br nanotubes.

	C8S3-Cl	**C8S3-Br**
Inner wall strongest coupling (cm^{-1})	1497.7	1462.5
	−1072.2	−1043.9
Outer wall strongest coupling (cm^{-1})	1509.9	1489
	−1044	−993.2
Interwall coupling (cm^{-1})	28.2	71.8
	−15.8	−39.8
Radius inner (nm)	3.55	6.47
Radius outer (nm)	6.5	8.61
Interwall distance (nm)	2.92	2.11

6.5.3 Time-Resolved Photoluminescence of C8S3-Br Nanotubes

PL decay maps were measured using a streak camera system with a synchro scan unit (Hamamatsu, model C5680) coupled to an inverted microscope. The excitation pulses were generated by focusing the output of a modelocked Ti:Sapphire (80 MHz, 150 fs) into a hollow fiber (Newport SCG-800) and subsequently selecting the excitation wavelength by a 530 ± 5 nm bandpass filter. A longpass dichroic mirror (DM) with the transmission edge at 550 nm directed the excitation beam towards a microfluidic flow-cell (micronit, The Netherlands) through which C8S3-Br sample solution was continuously pumped at a flowrate of $100\ \mu\mathrm{l\ h}^{-1}$. There the beam was focused by a $10\times$ objective (Melles Griot, $\mathrm{NA} = 0.26$). The intensity of the excitation beam was adjusted 2 µW (equivalent to about 1 absorbed photon per $\sim 1.6 \times 10^4$ molecules) to avoid exciton-exciton annihilation. The same objective collected the PL signal, which was transmitted by the DM to the backport of the microscope. A polarizer in magic angle configuration ensured that only lifetime decay is probed. Two 550 nm cutoff longpass filters were used to block residual excitation light that leaked through the DM. Experiments were conducted at room temperature.

A representative PL decay map for C8S3-Br nanotubes in solution is shown in Figure 6.7. Temporal integration of the PL decay map yields the steady-state spectrum (Figure 6.7, top panel), where two emission bands can clearly be identified. As a next step, one can spectrally integrate the area of each of the two emission bands separately in order to obtain the PL transients as depicted in the right panel of Figure 6.7.

If the two cylinders were strongly coupled, energy transfer from the high energy band 2 to the lower energy band 1 would reflect an additional loss channel for excited state population of band 2 leading to accelerated PL decay. Furthermore, as excited state population would be transferred from band 2 to band 1, the latter might show a delayed, in-growing PL intensity. As evident from the identical PL transients (rise times and decays) of both bands there is no significant energy transfer occurring on the timescale of the experiment, hence suggesting that the exciton population of both cylinders finds thermal equilibrium before decaying (non-)radiatively.

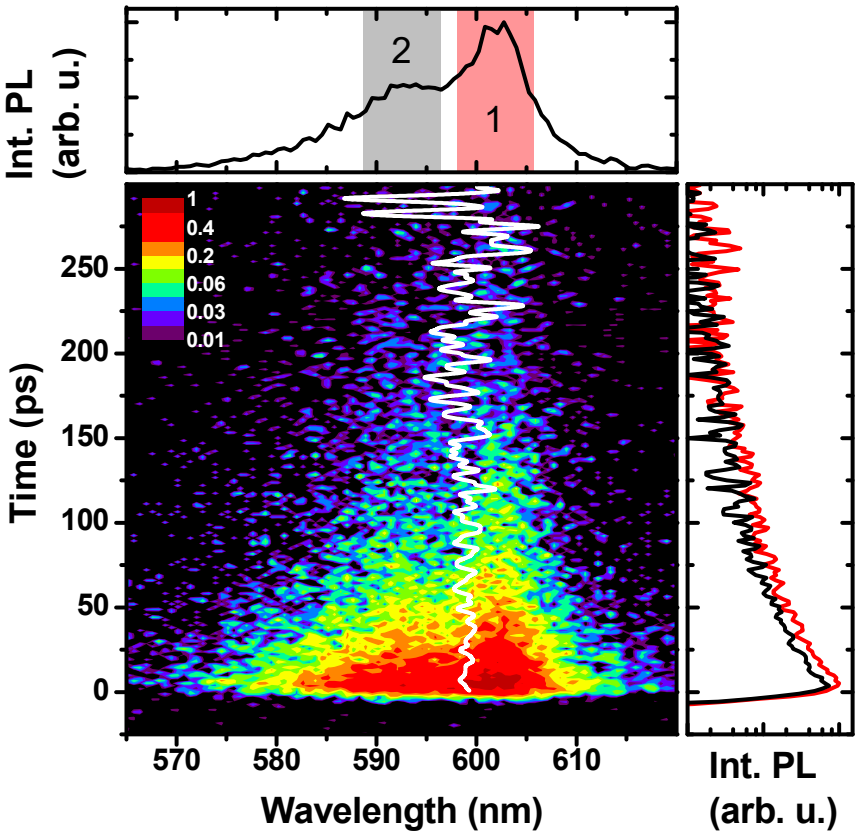

Figure 6.7. Center panel: PL decay map of C8S3-Br nanotubes in solution. PL intensity is depicted on a logarithmic color scale. The white line indicates the mean PL frequency at each time step. Upper panel: projection of the PL decay map along the time axis resulting in the steady-state PL spectrum. Right panel: transients obtained by integrating the PL map over the spectral intervals from 601 nm to 605 nm for band 1 (inner tube; red) and from 591 nm to 595 nm for band 2 (outer tube; black).

To further substantiate that no spectral diffusion is taking place we also computed the mean frequency $\langle \nu \rangle$ of the PL decay map as a function of time[50–52], depicted as a white line in Figure 6.7. We find that $\langle \nu \rangle$ remains constant, i.e., the white line is vertical in Figure 6.7 indicating thermal equilibrium transfer between band 1 and band 2. Note that for times > 200 ps the noise of $\langle \nu \rangle$ increases as the PL signal diminishes.

In conclusion, time-resolved PL measurements have shown that no significant population exchange occurs between the two cylinders on the timescale of photoluminescence emission. Therefore, we will treat the cylinder as separate (independent) species in our theoretical modelling.

6.5.4 Oxidation of C8S3-Br Nanotubes

The oxidation experiments are aimed at factorizing the contribution of the inner cylinder from the total absorption spectrum by impairing the outer cylinder absorption by silver nanoparticles[24,25,43]. Oxidation of C8S3-Br nanotubes was achieved by mixing 200 µl of the sample aggregate solution with 5.5 µl of $AgNO_3$ solution ($c = 10^{-2}$ M), gentle agitation and subsequent illumination for 60 s at roomlight[24]. The flask was then sealed and stored in the dark.

After 40 days of oxidation (much longer than for the C8S3-Cl nanotubes) distinct changes in the absorption spectrum were detected (Figure 6.8a, red and grey lines). The amplitude of the main peak at 592 nm that is associated with absorption of the outer cylinder, had strongly diminished relative to the lowest energy peak assigned to the inner wall absorption. Experimental evidence for the oxidation was obtained from cryo-TEM (Figure 6.8b and c), where silver clusters can be readily identified as black dots attached to the nanotubes. Both strongly and weakly oxidized nanotubes were observed. Therefore, a residual spectral signature of the outer cylinder is expected to be present in the absorption spectrum. This corresponds to the remaining (although strongly decreased) peak at 592 nm and the long shoulder at short wavelengths.

In order to ensure that over the extended oxidation period the observed spectral changes are not due to storage-related degradation, we recorded the absorption spectrum of the same pristine aggregate solution that was used for oxidation after two months. The corresponding spectrum shows only a slight decrease of the main peak relative to the lowest energy peak (Figure 6.8a, blue line) proving that oxidation indeed quenched the outer wall absorption.

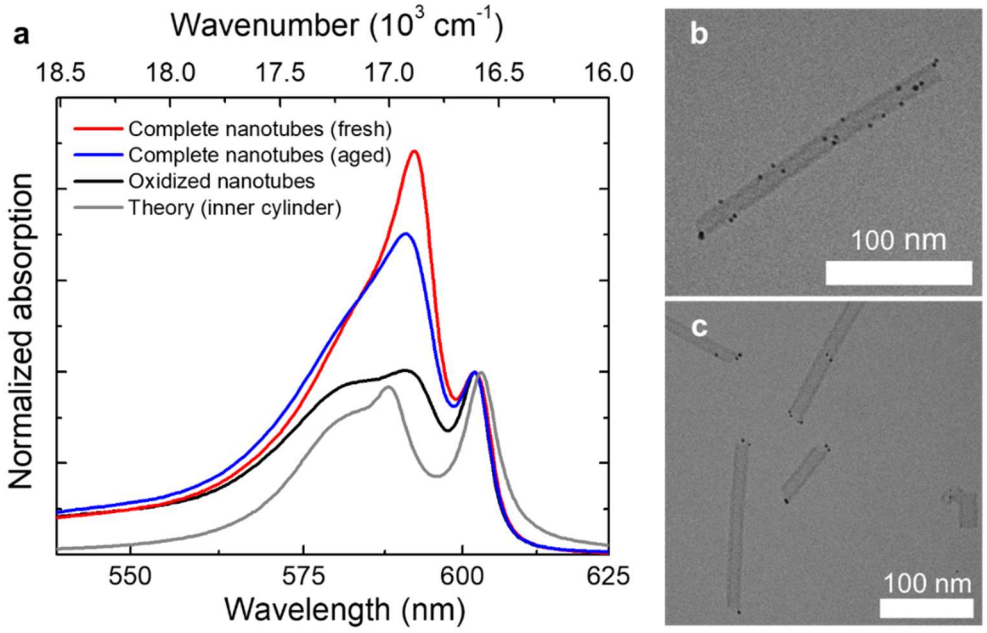

Figure 6.8. (a) Absorption spectrum of oxidized C8S3-Br nanotubes (solid black) in direct comparison to the spectrum of unoxidized (fresh) complete nanotubes (red), complete nanotubes after 2 months of storage (blue) and simulated spectrum of the inner cylinder (grey). All spectra were normalized to the amplitude of the lowest energy peak. On the right side, cryo-TEM micrographs of oxidized C8S3-Br nanotubes showing a high degree (b) and a low degree (c) of oxidation.

Bearing all these in mind, we compare the calculated spectrum of the inner cylinder (Figure 6.8a, grey line) with the spectrum of the oxidized nanotubes. The lowest energy peak at 602 nm that is associated with an optical transition of the inner cylinder, shows good agreement as well as the 580 nm centered band. This provides an additional support to the correctness of the spectral assignments of spectral signatures of the outer and inner cylinders.

6.5.5 Linear Dichroism of C8S3-Br Nanotubes

Dichroic absorption experiments were performed on a PerkinElmer Lambda 900 UV/VIS/NIR spectrometer with additional polarizer accessory (ASSY-L900). A peristaltic pump (Cole-Parmer Masterflex) and silicone tubing was used to flow-align the nanotubes in a flowcell (length: 38 mm, width: 8 mm, optical pathlength: 0.2 mm) at a flowrate of 2.5 ml s^{-1}. By illuminating the aligned sample with vertically or horizontally polarized light relative to the nanotube axis, polarization-dependent absorption were detected. The reduced linear dichroism was determined as outlined in Section 2.1.2.

A detailed description of the calculation of the theoretical LD spectrum can be found in the SI of the published paper[41]. In the experimental spectrum the orthogonal component ($OD_{\perp}$) of absorption was corrected by 10 % to align anisotropy below 500 nm at zero to account for small offsets in the baseline. It is important to note that the reduced linear dichroism is a pure measure of the polarization of optical transitions, where all other parameters (e.g. concentration and optical pathlength) fall out due to the normalization with the isotropic absorption spectrum (OD_{iso}). Therefore, not only the spectral shape, but also the amplitude of the obtained (experimentally and theoretically) spectra should be compared.

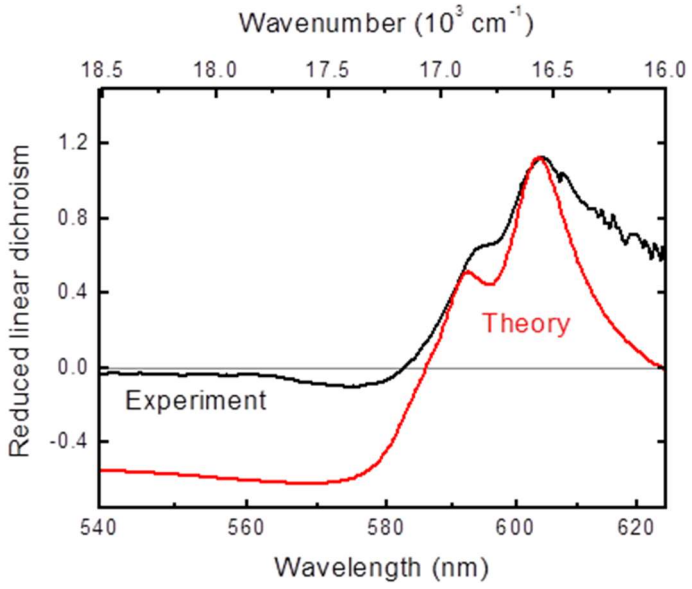

Figure 6.9. Experimental (solid black) and theoretical (solid red) reduced linear dichroism spectra for flow-aligned C8S3-Br nanotubes. The inset shows the relevant equation for the reduced linear dichroism as well as the limiting cases for completely parallel ($OD_{\perp} = 0$) and completely orthogonal ($OD_{||} = 0$) polarized transitions.

In a LD spectrum optical transitions that are polarized parallel to the nanotube axes will appear as positive features, whereas orthogonal polarized transitions lead to negative features. In close analogy to C8S3-Cl nanotubes, theory predicts that the two low energy peaks are polarized parallel to the

nanotube axis and therefore will show up as positive peaks in the LD spectrum. In contrast, the high energy tail is predominantly polarized orthogonal, such that a negative LD signal is expected.

The experimental and theoretical spectra show qualitative agreement (Figure 6.9), where all features are reproduced, i.e., a low energy peak around 603 nm, a shoulder at 594 nm corresponding to a peak at 592 nm in the theoretical spectrum and a negative dip at the tail below ~580 nm. The difference in the amplitudes of the negative signal between theory and experiment arises from denominator, i.e., the magnitude of the isotropic absorption. In experiment, absorption in this spectral region is partially due to non-aggregated molecules that are in an equilibrium with the nanotubes, which is not accounted for in theory. Hence, the theoretical isotropic spectrum underestimates the absorbance in this region leading to the overestimation of the negative tail in the LD spectrum.

6.5.6 Aggregation of C8S3-F

Addition of Milli-Q water to methanolic C8S3-F stock solution (Figure 6.10a) induces only minor changes to the spectrum (Figure 6.10b). The most pronounced new feature is a slightly red-shifted, weak peak at 554.5 nm. A prominent red-shift and narrowing of the absorption linewidth as is the case for C8S3-Br and C8S3-Cl molecules, were not observed under standard conditions of alcoholic route preparation[15]. The absence of significant spectral changes upon addition of water indicates that only minor aggregation occurs.

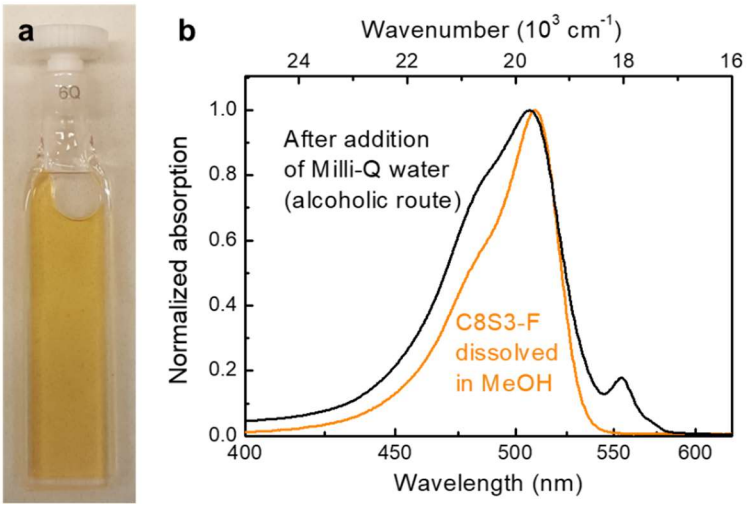

Figure 6.10. (a) Photograph of a cuvette with methanolic stock solution of C8S3-F. (b) Absorption spectrum of C8S3-F diluted in pure methanol (orange line) and after addition of Milli-Q water according to the alcoholic route (black line)[15].

6.5.7 Quantum Yield (QY)

Prior to QY measurements both methanolic stock solution of C8S3-Br as well as aggregate sample solutions were diluted to a peak optical density of ~0.1 in order to avoid PL reabsorption. PL spectra were recorded using a PerkinElmer LS50B Luminescence Spectrometer and 10 mm quartz cuvette (Starna GmbH, Germany). The quantum yield was calculated as outlined in Ref. [53]. The quantum yield C8S3-Br monomers dissolved in methanol was determined by comparison to rhodamine 6G in ethanol ($\Phi_s = 0.94 \pm 0.02$)[54], whereas for C8S3-Br nanotubes sulforhodamine 101 in ethanol ($\Phi_s = 0.95 \pm 0.03$)[55] was used as a reference. The excitation wavelength was chosen as 490 nm in case of monomers and 560 nm in case of nanotubes.

The PL quantum yield of C8S3-Br monomers in methanol and C8S3-Br nanotubes in aqueous solution were found to be 0.04 ± 0.01 (4 ± 1 %) in both cases with the error margin referring to the standard error upon averaging multiple independent measurements.

6.6 Author Contributions

B.K. performed the aggregate self-assembling and the optical experiments; their analysis was supervised by M.S.P. B.K. and L.E.F. performed the cryo-TEM experiments. A.S.B. performed the theoretical modeling and interpreted the optical spectra supervised by T.L.C.J. and J.K. V.R.J. performed the organic synthesis supervised by A.J.M. T.L.C.J., J.K., and M.S.P. conceived and developed the project. B.K., V.R.J., A.S.B., T.L.C.J., J.K., and M.S.P. wrote the paper.

6.7 References

1. Whitesides, G. M.; Grzybowski, B. Self-assembly at all scales. *Science* **295,** 2418–2421 (2002).
2. Hickey, R. J.; Koski, J.; Meng, X.; Riggleman, R. A.; Zhang, P.; Park, S.-J. Size-Controlled Self-Assembly of Superparamagnetic Polymersomes. *ACS Nano* **8,** 495–502 (2014).
3. Ghoroghchian, P. P.; Frail, P. R.; Susumu, K.; Blessington, D.; Brannan, A. K.; Bates, F. S.; Chance, B.; Hammer, D. A.; Therien, M. J. Near-infrared-emissive polymersomes: self-assembled soft matter for in vivo optical imaging. *Proc. Natl. Acad. Sci.* **102,** 2922–2927 (2005).
4. Howse, J. R.; Jones, R. A. L.; Battaglia, G.; Ducker, R. E.; Leggett, G. J.; Ryan, A. J. Templated formation of giant polymer vesicles with controlled size distributions. *Nat. Mater.* **8,** 507–511 (2009).
5. Hoeben, F. J. M.; Pascal Jonkheijm, P.; Meijer, E. W.; Schenning, A. P. H. J. About Supramolecular Assemblies of π-Conjugated Systems. *Chem. Rev.* **105,** 1491–1546 (2005).
6. Kaiser, T. E.; Wang, H.; Stepanenko, V.; Würthner, F. Supramolecular Construction of Fluorescent J-Aggregates Based on Hydrogen-Bonded Perylene Dyes. *Angew. Chemie Int. Ed.* **46,** 5541–5544 (2007).
7. Corradi, E.; Meille, S. V.; Messina, M. T.; Metrangolo, P.; Resnati, G. Halogen Bonding versus Hydrogen Bonding in Driving Self-Assembly Processes. *Angew. Chemie* **112,** 1852–1856 (2000).
8. Cavallo, G.; Metrangolo, P.; Milani, R.; Pilati, T.; Priimagi, A.; Resnati, G.; Terraneo, G. The Halogen Bond. *Chem. Rev.* **116,** 2478–2601 (2016).
9. Wang, C.; Wang, Z.; Zhang, X. Amphiphilic Building Blocks for Self-Assembly: From Amphiphiles to Supra-amphiphiles. *Acc. Chem. Res.* **45,** 608–618 (2012).
10. Sadownik, J. W.; Mattia, E.; Nowak, P.; Otto, S. Diversification of self-replicating molecules. *Nat. Chem.* **8,** 264–269 (2016).
11. van Dijken, D. J.; Chen, J.; Stuart, M. C. A.; Hou, L.; Feringa, B. L. Amphiphilic Molecular Motors for Responsive Aggregation in Water. *J. Am. Chem. Soc.* **138,** 660–669 (2016).
12. Ramanathan, M.; Shrestha, L. K.; Mori, T.; Ji, Q.; Hill, J. P.; Ariga, K. Amphiphile nanoarchitectonics: from basic physical chemistry to advanced applications. *Phys. Chem. Chem. Phys.* **15,** 10580–10611 (2013).
13. Du, J.; O'Reilly, R. K. Advances and challenges in smart and functional polymer vesicles. *Soft Matter* **5,** 3544–3561 (2009).
14. Spitz, C.; Knoester, J.; Ouart, A.; Daehne, S. Polarized absorption and anomalous temperature dependence of fluorescence depolarization in cylindrical J-aggregates. *Chem. Phys.* **275,** 271–284 (2002).
15. Didraga, C.; Pugžlys, A.; Hania, P. R.; von Berlepsch, H.; Duppen, K.; Knoester, J. Structure, spectroscopy, and microscopic model of tubular carbocyanine dye aggregates. *J. Phys. Chem. B* **108,** 14976–14985 (2004).
16. Würthner, F.; Kaiser, T. E.; Saha-Möller, C. R. J-Aggregates: From Serendipitous Discovery to Supramolecular Engineering of Functional Dye Materials. *Angew. Chemie Int. Ed.* **50,** 3376–3410 (2011).
17. Fidder, H.; Knoester, J.; Wiersma, D. A. Optical properties of disordered molecular aggregates: A numerical study. *J. Chem. Phys.* **95,** 7880 (1991).
18. Pawlik, A.; Ouart, A.; Kirstein, S.; Abraham, H.-W.; Daehne, S. Synthesis and UV/Vis Spectra of J-Aggregating 5, 5′, 6, 6′-Tetrachlorobenzimidacarbocyanine Dyes for Artificial Light-Harvesting Systems and for Asymmetrical Generation of Supramolecular Helices. *European J. Org. Chem.* **2003,** 3065–3080 (2003).
19. Kirstein, S.; Daehne, S. J-aggregates of amphiphilic cyanine dyes: Self-organization of artificial light harvesting complexes. *Int. J. Photoenergy* **2006,** 1–21 (2007).
20. von Berlepsch, H.; Ludwig, K.; Kirstein, S.; Böttcher, C. Mixtures of achiral amphiphilic cyanine dyes form helical tubular J-aggregates. *Chem. Phys.* **385,** 27–34 (2011).
21. Pawlik, A.; Kirstein, S.; De Rossi, U.; Daehne, S. Structural conditions for spontaneous generation of optical activity in J-aggregates. *J. Phys. Chem. B* **101,** 5646–5651 (1997).

22. De Rossi, U.; Moll, J.; Spieles, M.; Bach, G.; Daehne, S.; Kriwanek, J.; Lisk, M. Control of the J-Aggregation Phenomenon by variation of the N-alkyl-substituents. *J. für Prakt. Chemie/Chemiker-Zeitung* **337,** 203–208 (1995).
23. Abramavicius, D.; Nemeth, A.; Milota, F.; Sperling, J.; Mukamel, S.; Kauffmann, H. F. Weak exciton scattering in molecular nanotubes revealed by double-quantum two-dimensional electronic spectroscopy. *Phys. Rev. Lett.* **108,** 67401 (2012).
24. Eisele, D. M.; Cone, C. W.; Bloemsma, E. A.; Vlaming, S. M.; van der Kwaak, C. G. F.; Silbey, R. J.; Bawendi, M. G.; Knoester, J.; Rabe, J. P.; Vanden Bout, D. A. Utilizing redox-chemistry to elucidate the nature of exciton transitions in supramolecular dye nanotubes. *Nat. Chem.* **4,** 655–662 (2012).
25. Clark, K. A.; Cone, C. W.; Vanden Bout, D. A. Quantifying the Polarization of Exciton Transitions in Double-Walled Nanotubular J-Aggregates. *J. Phys. Chem. C* **117,** 26473–26481 (2013).
26. Eisele, D. M.; Arias, D. H.; Fu, X.; Bloemsma, E. A.; Steiner, C. P.; Jensen, R. A.; Rebentrost, P.; Eisele, H.; Tokmakoff, A.; Lloyd, S.; *et al.* Robust excitons inhabit soft supramolecular nanotubes. *Proc. Natl. Acad. Sci.* **111,** E3367–E3375 (2014).
27. Yuen-Zhou, J.; Arias, D. H.; Eisele, D. M.; Steiner, C. P.; Krich, J. J.; Bawendi, M. G.; Nelson, K. A.; Aspuru-Guzik, A. Coherent exciton dynamics in supramolecular light-harvesting nanotubes revealed by ultrafast quantum process tomography. *ACS Nano* **8,** 5527–5534 (2014).
28. Megow, J.; Röhr, M. I. S.; Schmidt am Busch, M.; Renger, T.; Mitrić, R.; Kirstein, S.; Rabe, J. P.; May, V. Site-dependence of van der Waals interaction explains exciton spectra of double-walled tubular J-aggregates. *Phys. Chem. Chem. Phys.* **17,** 6741–6741 (2015).
29. Caram, J. R.; Doria, S.; Eisele, D. M.; Freyria, F. S.; Sinclair, T. S.; Rebentrost, P.; Lloyd, S.; Bawendi, M. G. Room-Temperature Micron-Scale Exciton Migration in a Stabilized Emissive Molecular Aggregate. *Nano Lett.* **16,** 6808–6815 (2016).
30. Cogdell, R. J.; Gardiner, A. T.; Hashimoto, H.; Brotosudarmo, T. H. P. A comparative look at the first few milliseconds of the light reactions of photosynthesis. *Photochem. Photobiol. Sci.* **7,** 1150–1158 (2008).
31. Ganapathy, S.; Oostergetel, G. T.; Wawrzyniak, P. K.; Reus, M.; Chew, A. G. M.; Buda, F.; Boekema, E. J.; Bryant, D. A.; Holzwarth, A. R.; de Groot, H. J. M. Alternating syn-anti bacteriochlorophylls form concentric helical nanotubes in chlorosomes. *Proc. Natl. Acad. Sci.* **106,** 8525–8530 (2009).
32. McConnell, I.; Li, G.; Brudvig, G. W. Energy conversion in natural and artificial photosynthesis. *Chem. Biol. Rev.* **17,** 434–447 (2010).
33. Orf, G. S.; Blankenship, R. E. Chlorosome antenna complexes from green photosynthetic bacteria. *Photosynth. Res.* **116,** 315–331 (2013).
34. Günther, L. M.; Jendrny, M.; Bloemsma, E. A.; Tank, M.; Oostergetel, G. T.; Bryant, D. A.; Knoester, J.; Köhler, J. Structure of Light-Harvesting Aggregates in Individual Chlorosomes. *J. Phys. Chem. B* **120,** 5367–5376 (2016).
35. von Berlepsch, H.; Kirstein, S.; Hania, R.; Pugžlys, A.; Böttcher, C. Modification of the nanoscale structure of the J-aggregate of a sulfonate-substituted amphiphilic carbocyanine dye through incorporation of surface-active additives. *J. Phys. Chem. B* **111,** 1701–1711 (2007).
36. von Berlepsch, H.; Kirstein, S.; Böttcher, C. Effect of alcohols on J-aggregation of a carbocyanine dye. *Langmuir* **18,** 7699–7705 (2002).
37. von Berlepsch, H.; Kirstein, S.; Böttcher, C. Supramolecular structure of J-aggregates of a sulfonate substituted amphiphilic carbocyanine dye in solution: Methanol-induced ribbon-to-tubule transformation. *J. Phys. Chem. B* **108,** 18725–18733 (2004).
38. Vlaming, S. M.; Bloemsma, E. A.; Nietiadi, M. L.; Knoester, J. Disorder-induced exciton localization and violation of optical selection rules in supramolecular nanotubes. *J. Chem. Phys.* **134,** 114507 (2011).
39. Clark, K. A.; Krueger, E. L.; Vanden Bout, D. A. Direct measurement of energy migration in supramolecular carbocyanine dye nanotubes. *J. Phys. Chem. Lett.* **5,** 2274–2282 (2014).
40. Chuang, C.; Lee, C. K.; Moix, J. M.; Knoester, J.; Cao, J. Quantum Diffusion on Molecular Tubes: Universal Scaling of the 1D to 2D Transition. *Phys. Rev. Lett.* **116,** 196803 (2016).
41. Kriete, B.; Bondarenko, A. S.; Jumde, V. R.; Franken, L. E.; Minnaard, A. J.; Jansen, T. L. C.; Knoester, J.; Pshenichnikov, M. S. Steering Self-Assembly of Amphiphilic Molecular Nanostructures via Halogen Exchange. *J. Phys. Chem. Lett.* **8,** 2895–2901 (2017).
42. Didraga, C.; Klugkist, J. A.; Knoester, J. Optical Properties of Helical Cylindrical Molecular Aggregates: The Homogeneous Limit. *J. Phys. Chem. B* **106,** 11474–11486 (2002).
43. Eisele, D. M.; von Berlepsch, H.; Böttcher, C.; Stevenson, K. J.; Vanden Bout, D. A.; Kirstein, S.; Rabe, J. P. Photoinitiated growth of sub-7 nm silver nanowires within a chemically active organic nanotubular template. *J. Am. Chem. Soc.* **132,** 2104–2105 (2010).
44. Steeg, E.; Kirmse, H.; Rabe, J. P.; Kirstein, S. Silver iodide nanowires grown within tubular J-aggregates. *J. Colloid Interface Sci.* **530,** 424–432 (2018).
45. Bloemsma, E. A.; Vlaming, S. M.; Malyshev, V. A.; Knoester, J. Signature of Anomalous Exciton Localization in the Optical Response of Self-Assembled Organic Nanotubes. *Phys. Rev. Lett.* **114,** 156804 (2015).
46. Didraga, C.; Knoester, J. Optical spectra and localization of excitons in inhomogeneous helical cylindrical aggregates. *J. Chem. Phys.* **121,** 10687 (2004).

47. Friedl, C.; Renger, T.; von Berlepsch, H.; Ludwig, K.; Schmidt am Busch, M.; Megow, J. Structure Prediction of Self-Assembled Dye Aggregates from Cryogenic Transmission Electron Microscopy, Molecular Mechanics, and Theory of Optical Spectra. *J. Phys. Chem. C* **120,** 19416–19433 (2016).
48. Czikkely, V.; Försterling, H. D.; Kuhn, H. Light absorption and structure of aggregates of dye molecules. *Chem. Phys. Lett.* **6,** 11–14 (1970).
49. Jorgensen, W. L.; Severance, D. L. Aromatic-aromatic interactions: free energy profiles for the benzene dimer in water, chloroform, and liquid benzene. *J. Am. Chem. Soc.* **112,** 4768–4774 (1990).
50. Bawendi, M. G.; Carroll, P. J.; Wilson, W. L.; Brus, L. E. Luminescence properties of CdSe quantum crystallites: Resonance between interior and surface localized states. *J. Chem. Phys.* **96,** 946 (1992).
51. Kagan, C. R.; Murray, C. B.; Bawendi, M. G. Long-range resonance transfer of electronic excitations in close-packed CdSe quantum-dot solids. *Phys. Rev. B* **54,** 8633–8643 (1996).
52. Crooker, S. A.; Hollingsworth, J. A.; Tretiak, S.; Klimov, V. I. Spectrally Resolved Dynamics of Energy Transfer in Quantum-Dot Assemblies: Towards Engineered Energy Flows in Artificial Materials. *Phys. Rev. Lett.* **89,** 186802 (2002).
53. Würth, C.; Grabolle, M.; Pauli, J.; Spieles, M.; Resch-Genger, U. Comparison of Methods and Achievable Uncertainties for the Relative and Absolute Measurement of Photoluminescence Quantum Yields. *Anal. Chem.* **83,** 3431–3439 (2011).
54. Kubin, R. F.; Fletcher, A. N. Fluorescence quantum yields of some rhodamine dyes. *J. Lumin.* **27,** 455–462 (1982).
55. Brouwer, A. M. Standards for photoluminescence quantum yield measurements in solution (IUPAC Technical Report). *Pure Appl. Chem.* **83,** 2213–2228 (2011).

[This page was intentionally left blank]